Giant magnetic moment enhancement of nickel nanoparticles embedded in multiwalled carbon nanotubes

Jun Wang,[1] Pieder Beeli,[2] Yang Ren,[3] and Guo-meng Zhao[1,2,*]
[1]*Department of Physics, Faculty of Science, Ningbo University, Ningbo, People's Republic of China*
[2]*Department of Physics and Astronomy, California State University, Los Angeles, California 90032, USA*
[3]*X-Ray Science Division, Advance Photon Source, Argonne National Laboratory, Argonne, Illinois 60439, USA*
(Received 1 October 2010; published 19 November 2010)

We report a giant magnetic moment enhancement of ferromagnetic nickel nanoparticles (11 nm) embedded in multiwalled carbon nanotubes (MWCNTs). High-energy synchrotron x-ray diffraction experiment and chemical analysis are used to accurately determine the ferromagnetic nickel concentration. Magnetic measurements show that the room-temperature saturation magnetization of the nickel nanoparticles embedded in the MWCNTs is enhanced by a factor of about 3.4 ± 1.0 as compared with what they would be expected to have for free nanoparticles. The giant moment enhancement is unlikely to be explained by a magnetic proximity effect but possibly arise from the interplay between ferromagnetism in nickel nanoparticles and strong diamagnetism in multiwalled carbon nanotubes.

DOI: 10.1103/PhysRevB.82.193410 PACS number(s): 75.50.Tt, 61.48.De, 81.05.U−

Graphene is a sheet of carbon atoms distributed in a honeycomb lattice and is the building block for carbon-based materials such as graphite and carbon nanotubes. The massless relativistic Dirac fermions in graphene are a result of its unique electronic structure, characterized by conical valence and conduction bands that meet at a single point in momentum space. The integer quantum-Hall effect recently observed in graphene[1,2] is related to the Dirac fermions. More intriguingly, there are reports of ultrahigh-temperature superconducting behaviors in both graphite[3] and graphite-sulfur composites.[4,5] Highly oriented pyrolithic graphite (HOPG) has been shown to display either a partial superconducting or a ferromagneticlike response to an applied magnetic field even at temperatures well above room temperature.[3] In addition to the observation of unusual high-temperature ferromagnetism in the carbon-based materials,[6–8] there is a report of extra magnetic moment induced in graphite due to a large magnetic proximity effect (MPE) between graphite and magnetic nanoparticles.[9] However, this important conclusion strongly depends on whether the magnetic impurity concentrations inferred from Mössbauer spectra[9] are accurate enough.

Here we study magnetic properties of multiwalled carbon nanotubes (MWCNTs) embedded with ferromagnetic Ni nanoparticles. Because Ni nanoparticles sit inside the innermost shells of MWCNTs [see Fig. 1(c) below] and electronic intershell coupling is negligibly small, we expect that the only shells that can interact with the Ni nanoparticles are the innermost shells. Then the extra magnetic moments induced by the MPE should be much smaller than those found in graphite.[9] However, our data show a giant magnetic moment enhancement that is about two orders of magnitude larger than that predicted from the MPE.

Purified MWCNT mat samples (Lot No. TS0636) from SES Research of Houston were synthesized by chemical-vapor deposition under catalyzation of nickel nanoparticles. Some of nickel nanoparticles got into the nanotubes during the nanotube growth. After purification of as-grown MWCNT mat samples, most nickel nanoparticles were removed except for those embedded inside the innermost shells. The macroscopic samples used for the different measurements or analyses described below are from the same batch, which should be identical. The morphology of the mat

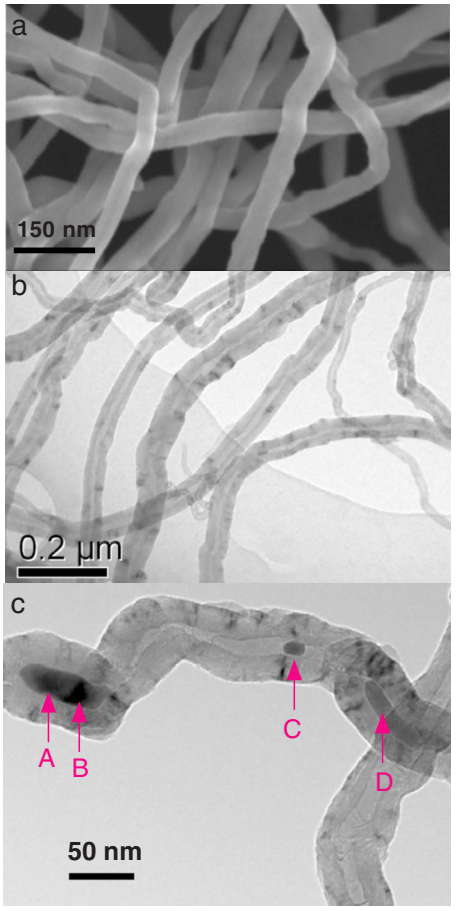

FIG. 1. (Color online) (a) SEM image of a Ni-filled MWCNT mat sample. (b) TEM image of a Ni-filled MWCNT mat sample. (c) TEM image of a selected MWCNT filled with nickel nanoparticles labeled by A, B, C, and D.

sample can be seen from scanning electron microscopy (SEM) image shown in Fig. 1(a). The SEM image was taken by a field-emission scanning electron microcopy (FE-SEM, Hitachi S-4800) using an accelerating voltage of 3 kV. One can see that the outer diameters of these MWCNTs are in the range of 30–50 nm and centered around 40 nm. The mean inner diameter of the MWCNTs is about 10 nm, as seen from the transmission electron microscopy (TEM) images [Figs. 1(b) and 1(c)] recorded by FEI Tecnai F20 with an accelerating voltage of 200 kV. The nickel nanoparticles sit inside the innermost shells near the ends of the tubes, as labeled by A, B, C, and D in Fig. 1(c). Some nickel nanoparticles are connected to form a continuous chain [see a location labeled by D in Fig. 1(c)].

The total metal-based impurity concentrations of the mat sample can be determined from the composition analysis of the residual of the sample, which was obtained by burning off carbon-based materials in air. A Perkin-Elmer Elan-DRCe inductively coupled plasma mass spectrometer (ICP-MS) was used to analyze the composition of the residual. From the weight (1.33%) of the residual and the ICP-MS analysis, we obtain the metal-based magnetic impurity concentrations in weight: Ni=0.476%, Fe=0.00907%, and Co=0.0133%.

In order to quantitatively understand the magnetism of the Ni-filled MWCNTs, it is essential to determine the concentration of the ferromagnetic nickel phase. We can achieve this goal by performing high-energy synchrotron x-ray diffraction (XRD) experiment. Figure 2(a) shows a synchrotron XRD spectrum for a virgin Ni-filled MWCNT sample. The XRD spectrum was taken on a high-energy synchrotron x-ray beamline 11-ID-C at the Advanced Photon Source, Argonne National Laboratory, using monochromated radiation with a wavelength of $\lambda=0.1078$ Å. The major peaks in the spectrum of Fig. 2(a) correspond to the diffraction peaks of MWCNT (Ref. 10) and the face-centered cubic (fcc) phase of Ni. In particular, the (002) diffraction peak of MWCNT is seen at $2\theta=1.815°$ and the Ni (311) peak at $2\theta=5.815°$. Figure 2(b) displays the expanded view of the Ni (311) peak. The solid line is the fitted curve by a Gaussian. The integrated intensity of the Ni (311) peak is found to be $0.84\pm0.08\%$ of the intensity of the MWCNT (002) peak. Using the calculated standard intensities of the graphite (002) and Ni (311) peaks and assuming that the intensity of MWCNT (002) peak is the same as that of graphite (002), we find that the ferromagnetic fcc nickel concentration is $0.43\pm0.04\%$ (in weight), which is slightly lower than the total Ni concentration (0.476%) inferred from ICP-MS. This implies that the ferromagnetic fcc nickel is the dominant phase while the concentrations of other nonmagnetic nickel-based phases are too small to be seen in the XRD spectrum.

In order to check the reliability of our inferred ferromagnetic nickel concentration based on the Ni (311) peak, we show, in Fig. 2(c), the expected XRD spectrum of the fcc Ni with the concentration of 0.43% [lower curve in Fig. 2(c)] and the difference spectrum [upper curve in Fig. 2(c)], which is obtained by subtracting the Ni spectrum from the spectrum of Ni-filled MWCNT sample in Fig. 2(a). The difference spectrum shows no observable residual of any peaks of the fcc nickel, implying that the inferred Ni concentration is indeed reliable. Furthermore, all the peaks except for some

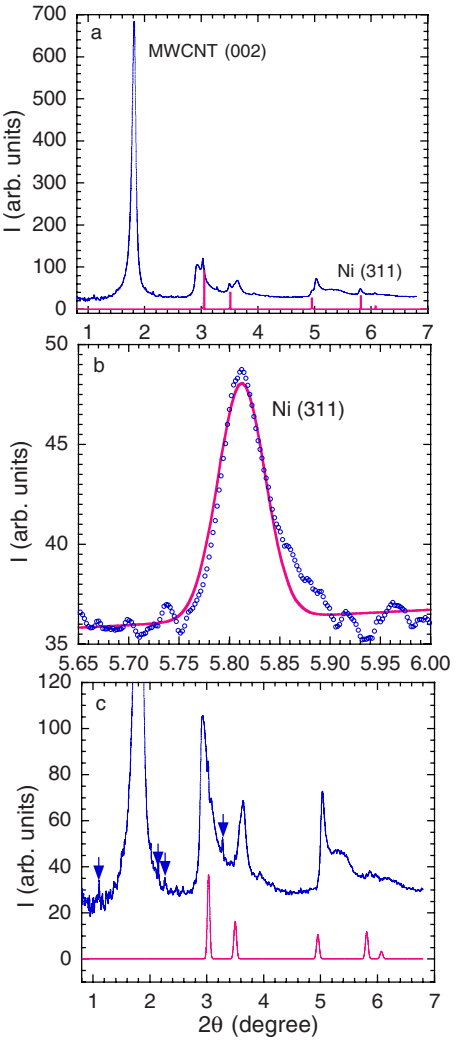

FIG. 2. (Color online) (a) High-energy synchrotron XRD spectrum for a virgin Ni-filled MWCNT sample (upper curve) and the standard spectrum for fcc nickel (lower curve). (b) The expanded view of the Ni (311) peak. (c) The expected XRD spectrum of the fcc Ni (lower curve) based on the nickel concentration (0.43%) and the difference spectrum (upper curve), which is obtained by subtracting the Ni spectrum from the spectrum of Ni-filled MWCNT sample in Fig. 2(a).

peaks indicated by arrows in the difference spectrum agree with the peaks observed in pure MWCNTs.[10] The extra peaks indicated by the arrows should be associated with other impurity phases.

Since magnetic properties of nanoparticles depend strongly on the particle size, it is important to determine the average diameter d of the ferromagnetic Ni nanoparticles embedded in MWCNTs. We can determine d from the peak width of the XRD spectrum. The full width at half maximum of the Ni (311) peak is found to be 0.0556° from the Gaussian fit in Fig. 2(b). Using the Scherrer equation:[11] $d=0.89\lambda/(\beta\cos\theta)$ and with $\beta=0.0511°$ (after correcting for the instrumental broadening), we calculate $d=11$ nm, in good agreement with the average inner diameter of the tubes [see Fig. 1(b)].

With the information of the average diameter (11 nm) of

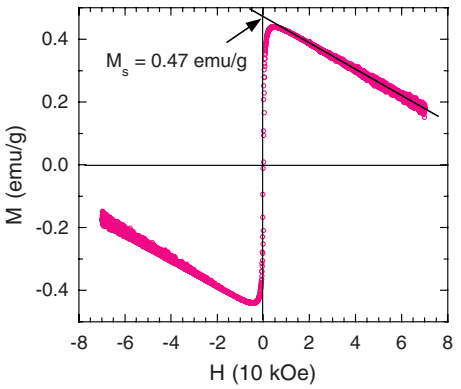

FIG. 3. (Color online) Magnetic hysteresis loop of a Ni-filled MWCNT mat sample at 320 K.

the ferromagnetic Ni nanoparticles and its concentration of 0.43% in our Ni-filled MWCNT sample, we would expect the room-temperature saturation magnetization (M_s) to be 0.14 emu/g from the known M_s=30–32 emu/g for pure fcc Ni nanoparticles with d=11–12 nm (Ref. 12). If we use the upper limit of M_s=55 emu/g for bulk Ni, the expected M_s for our Ni-filled MWCNT sample would be 0.24 emu/g. Figure 3 shows magnetization versus magnetic field for our Ni-filled MWCNT mat sample at 320 K (the sample mass is 5.75 mg). The magnetization was measured using a Quantum Design vibrating sample magnetometer (VSM) and the magnitude of the magnetization is repeatable with less than 10% uncertainty. The linear field dependence of the magnetization with a negative slope at $H>10$ kOe is due to the diamagnetic contribution. The linear extrapolation to $H=0$ yields $|\chi_{dia}|=4.2\times10^{-6}$ emu/g and M_s=0.47 emu/g. The measured M_s value is a factor of 3.4 larger than the expected value (0.14 emu/g) from the measured Ni concentration and average diameter. Considering 10% uncertainty for the nickel concentration, 10% uncertainty for the magnetization, and 25% uncertainty for the expected saturation magnetization of the free nickel nanoparticles, we estimate the moment enhancement factor to be 3.4 ± 1.0. Thus, there is a giant magnetic moment enhancement of the Ni nanoparticles when they are embedded inside the innermost shells of MWCNTs. Using the measured nickel concentration (0.43%), the enhanced saturation magnetization ΔM_s is calculated to be about 76.7 emu/g of nickel or 683 emu/cc of nickel.

If the observed giant magnetic moment enhancement arises from the magnetic proximity effect, then as proposed in Ref. 9, there should exist two distinctive ferromagneticlike transitions. Figure 4(a) shows zero-field-cooled (ZFC) and FC magnetic susceptibilities of another virgin Ni-filled MWCNT sample in a field of 100 Oe. We clearly see that there is only one ferromagnetic transition at about 630 K and the FC susceptibility below T_C is significantly larger than the ZFC susceptibility. For comparison, Fig. 4(b) shows the ZFC and FC susceptibilities for pure nickel powders (obtained from Shanghai Chemical Regent Co., China). The mean diameter of the Ni crystallites (subparticles) is calculated to be about 46 nm from the width of the XRD (311) peak. Within the experimental uncertainty, the Curie temperature of the pure nickel powders is close to that of the nickel nanoparticles embedded in MWCNTs.

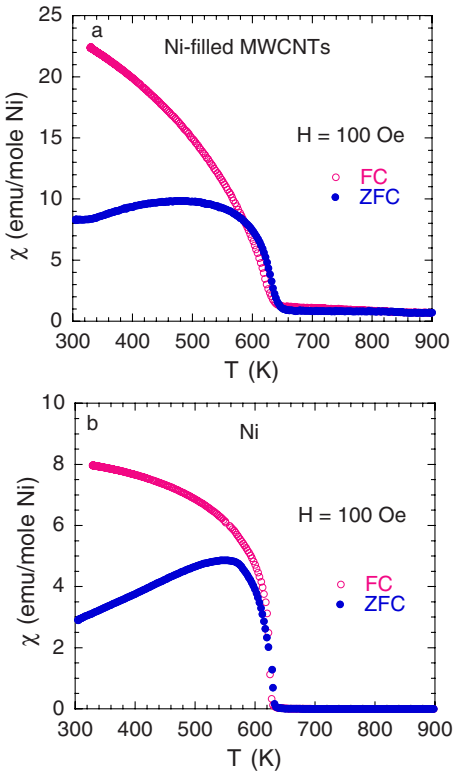

FIG. 4. (Color online) (a) ZFC and FC magnetic susceptibilities of a virgin Ni-filled MWCNT mat sample in a field of 100 Oe. (b) ZFC and FC susceptibilities for pure nickel powders.

Now we turn to discuss the origin of the giant magnetic moment enhancement of the nickel nanoparticles embedded in MWCNTs. One possibility is that this enhancement arises from a large magnetic proximity effect.[9,13] We consider a simple case where our ferromagnetic nanoparticles have a cylindrical shape with both length and diameter equal to d and the curve surface of the cylinder contacts with the innermost shell of a MWCNT (this is the most favorable case for the proximity effect). The curved surface area is equal to πd^2 and the total number of the contact carbon is $\pi N_c d^2$, where N_c is the number of carbon per unit area and equal to $3.82\times10^{15}/\mathrm{cm}^2$ (Ref. 14). If the induced magnetic moment is $m\mu_B$ (where μ_B is the Bohr magneton) per contact carbon atom, then the induced saturation magnetization normalized to the volume of the ferromagnetic nanoparticle is $\Delta M_s = 4N_c m\mu_B/d = 1420(m/d)$ emu/cm^3 (here d is in units of nanometer). Using the measured ΔM_s=683 emu/cm^3 and d=11 nm for ferromagnetic nickel nanoparticles, we find that m=5.3, which is a factor of 53 larger than the value ($\sim$0.1) calculated using density-functional theory.[13] Therefore, the magnetic proximity model seems unlikely to explain such a giant magnetic moment enhancement.

Alternatively, it is possible that a strong diamagnetic tube could enhance the extrinsic magnetic moment of a (single-domain) magnet embedded inside it. If the tube were a perfect diamagnet, the "poles" of the magnet would be extended further apart (to the length of the tube) without changing their strength, thus giving an extrinsic enhancement to the magnetic moment. This is because the perfect diamagnetism of the tube prevents the magnetic field lines of the magnet

from leaking out through the wall of the tube.

The plausibility of this interpretation depends on whether MWCNTs would exhibit strong diamagnetism when the magnetic field is applied in the tube-axis direction. Since the orbital diamagnetism for the field parallel to the tube-axis direction is negligibly small, one of possible origins for strong diamagnetism would be superconductivity. The observation of superconductinglike hysteresis loops in HOPG at 400 K would be a good indication of local superconductivity well above room temperature.[3] Based on resonating-valence-bond theory originally proposed by Anderson,[15] Black-Schaffer, and Doniach[16] have recently shown that heavily doped graphene would exhibit *d*-wave ultrahigh-temperature superconductivity.[16] If such ultrahigh-temperature superconductivity would also exist in MWCNTs, the giant enhancement in the saturation magnetization would be naturally explained. Further experiments on well-controlled samples are required to check if the magnetic properties of MWCNTs would be consistently explained in terms of *d*-wave ultrahigh temperature superconductivity.

We thank M. Du and F. M. Zhou for the elemental analyses using ICP-MS. We also thank the Palmdale Institute of Technology for the use of the VSM. Use of the Advanced Photon Source was supported by the U.S. Department of Energy, Office of Science, Office of Basic Energy Sciences, under Contract No. DE-AC02-06CH11357. This work was supported by the National Natural Science Foundation of China (Grant No. 10874095), the Science Foundation of China, Zhejiang (Grants No. Y407267 and No. 2009C31149), the Natural Science Foundation of Ningbo (Grants No. 2008B10051 and No. 2009B21003), K. C. Wong Magna Foundation, and Y. G. Bao's Foundation.

*gzhao2@calstatela.edu

[1] K. S. Novoselov, A. K. Geim, S. V. Morozov, D. Jiang, M. I. Katsnelson, I. V. Grigorieva, S. V. Dubonos, and A. A. Firsov, Nature (London) **438**, 197 (2005).

[2] Y.-B. Zhang, Y.-W. Tan, H. L. Stormer, and P. Kim, Nature (London) **438**, 201 (2005).

[3] Y. Kopelevich, P. Esquinazi, J. H. S. Torres, and S. Moehlecke, J. Low Temp. Phys. **119**, 691 (2000).

[4] R. R. da Silva, J. H. S. Torres, and Y. Kopelevich, Phys. Rev. Lett. **87**, 147001 (2001).

[5] S. Moehlecke, Y. Kopelevich, and M. B. Maple, Phys. Rev. B **69**, 134519 (2004).

[6] A. W. Mombru, H. Pardo, R. Faccio, O. F. de Lima, E. R. Leite, G. Zanelatto, A. J. C. Lanfredi, C. A. Cardoso, and F. M. Araujo-Moreira, Phys. Rev. B **71**, 100404(R) (2005).

[7] P. Esquinazi, D. Spemann, R. Hohne, A. Setzer, K. H. Han, and T. Butz, Phys. Rev. Lett. **91**, 227201 (2003).

[8] J. Červenka, M. I. Katsnelson, and C. F. J. Flipse, Nat. Phys. **5**, 840 (2009).

[9] J. M. D. Coey, M. Venkatesan, C. B. Fitzgerald, A. P. Douvalis, and I. S. Sanders, Nature (London) **420**, 156 (2002).

[10] D. Reznik, C. H. Olk, D. A. Neumann, and J. R. D. Copley, Phys. Rev. B **52**, 116 (1995).

[11] H. P. Klug and L. E. Alexander, *X-ray Diffraction Procedures for Polycrystalline and Amorphous Materials*, 2nd ed. (Wiley Interscience, New York, 1974), p. 689.

[12] D. H. Chen and C. H. Hsieh, J. Mater. Chem. **12**, 2412 (2002); W. Gong, H. Li, Z. Zhao, and J. Chen, J. Appl. Phys. **69**, 5119 (1991).

[13] O. Céspedes, M. S. Ferreira, S. Sanvito, M. Kociak, and J. M. D. Coey, J. Phys.: Condens. Matter **16**, L155 (2004).

[14] P. R. Wallace, Phys. Rev. **71**, 622 (1947).

[15] P. W. Anderson, Science **235**, 1196 (1987).

[16] A. M. Black-Schaffer and S. Doniach, Phys. Rev. B **75**, 134512 (2007).